AD-A055 246 COLD REGIONS RESEARCH AND ENGINEERING LAB HANOVER N H F/G 8/12
THE COMPRESSION OF WET SNOW,(U)
APR 78 S C COLBECK, K A SHAW, G LEMIEUX

UNCLASSIFIED CRREL-78-10 NL

| OF |
AD
A055246

END
DATE
FILMED
7-78
DDC

CRREL
REPORT 78-10

FOR FURTHER TRANSFER

12

The compression of wet snow

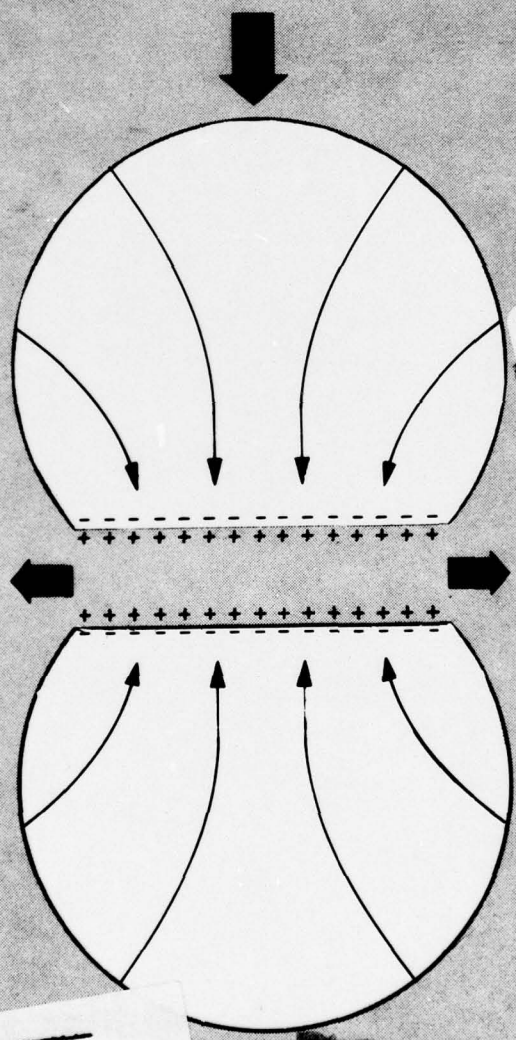

Cover: Interparticle forces cause heat flow, pressure melting, metlwater flow, and double charged layers.

CRREL Report 78-10

The compression of wet snow

S.C. Colbeck, K.A Shaw and G. Lemieux

April 1978

Prepared for
DIRECTORATE OF FACILITIES ENGINEERING
OFFICE, CHIEF OF ENGINEERS
By
CORPS OF ENGINEERS, U.S. ARMY
COLD REGIONS RESEARCH AND ENGINEERING LABORATORY
HANOVER, NEW HAMPSHIRE

Unclassified

SECURITY CLASSIFICATION OF THIS PAGE (When Data Entered)

REPORT DOCUMENTATION PAGE

READ INSTRUCTIONS BEFORE COMPLETING FORM

1. REPORT NUMBER: CRREL Report 78-10
2. GOVT ACCESSION NO.
3. RECIPIENT'S CATALOG NUMBER: (14) CRREL-78-10

4. TITLE (and Subtitle): (6) THE COMPRESSION OF WET SNOW
5. TYPE OF REPORT & PERIOD COVERED
6. PERFORMING ORG. REPORT NUMBER

7. AUTHOR(s): (10) S.C. Colbeck, K.A. Shaw and G. Lemieux
8. CONTRACT OR GRANT NUMBER(s): (17) A3, E1

9. PERFORMING ORGANIZATION NAME AND ADDRESS
U.S. Army Cold Regions Research and Engineering Laboratory
Hanover, New Hampshire 03755

10. PROGRAM ELEMENT, PROJECT, TASK AREA & WORK UNIT NUMBERS
(16) DA Project 4A161102AT24
Task A3 and E1, Work Unit 001

11. CONTROLLING OFFICE NAME AND ADDRESS
Directorate of Facilities Engineering
Office, Chief of Engineers
Washington, D.C. 20314

12. REPORT DATE: (11) April 1978
13. NUMBER OF PAGES: 23

14. MONITORING AGENCY NAME & ADDRESS (if different from Controlling Office): (12) 25 p.

15. SECURITY CLASS. (of this report): Unclassified
15a. DECLASSIFICATION/DOWNGRADING SCHEDULE

16. DISTRIBUTION STATEMENT (of this Report)

Approved for public release; distribution unlimited.

17. DISTRIBUTION STATEMENT (of the abstract entered in Block 20, if different from Report)

18. SUPPLEMENTARY NOTES

ABSTRACT

19. KEY WORDS (Continue on reverse side if necessary and identify by block number)
Compressibility
Liquids
Salinity
Viscous deformation
Wet snow

20. ABSTRACT (Continue on reverse side if necessary and identify by block number)

The compressibility of wet snow is described in terms of pressure melting and nonlinear viscous deformation at grain contacts. The results of experiments with different salinities and liquid water contents are compared with computed densities. The decreasing compressibility of wet snow with increasing salinity and decreasing liquid content is quantified and explained. Simultaneous particle growth and the doubly charged layer at phase boundaries are included in the model. The results show that the density of wet snow increases approximately as a power of time but is highly dependent on the stress, initial particle size, liquid water content, and ionic impurity content of the snow.

037 700

DD FORM 1 JAN 73 1473 EDITION OF 1 NOV 65 IS OBSOLETE

ABSTRACT

Unclassified

SECURITY CLASSIFICATION OF THIS PAGE (When Data Entered)

PREFACE

This study was conducted and this report was prepared by Dr. S.C. Colbeck, Geophysicist, K.A. Shaw, Research Assistant, and G. Lemieux, Physicist, of the Snow and Ice Branch, Research Division, U.S. Army Cold Regions Research and Engineering Laboratory.

The work was funded under DA Project 4A161102AT24, *Research in Snow, Ice and Frozen Ground;* Task A3, *Research in Terrain and Climatic Constraints* and Task E1, *Cold Environmental Factors;* Work Unit 001, *Research in Snow Mechanics.*

The technical content of this report was reviewed by Dr. W.F. St. Lawrence and Dr. K.F. Sterrett of CRREL.

The authors would like to thank Dr. G.D. Ashton and Dr. W.F. St. Lawrence for their comments and encouragement during the period of this study. They also gratefully acknowledge the suggestions of Dr. Sterrett, and Dr. D. Tabor of Cavendish Laboratory, Cambridge University, concerning the significance of the double charged layer.

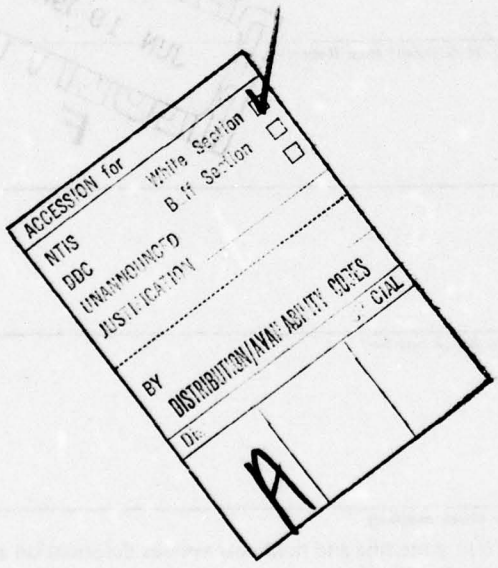

CONTENTS

ILLUSTRATIONS

TABLES

NOMENCLATURE

A	coefficient
A_f	average area of face of a cell containing one particle
C_b	concentration of dissolved air at bond
C_s	concentration of dissolved air in pore water
d	thickness of liquid film
D	displacement of melt surface
D_i	diffusion coefficient
f_i	fraction of particles with radius r_i
F	force between particles
h	height of melt cap
I	number of dissociated ions per molecule
k_i	thermal conductivity of ice
L	latent heat of fusion
m	exponent
n	number of stressed contacts per particle
N	total number of particles
N_0	initial number of particles
N_s	number of shrinking particles
p_c	capillary pressure, air pressure minus liquid pressure
r	radial coordinate
r_a	air bubble radius
r_b	bond radius
r_i	particle radius
r_0	initial particle radius
r_p	particle radius
$\bar{r}$	average particle radius
R	gas constant
r_τ	particle radius at time τ
S_b	concentration of dissolved salt at bond
S_s	concentration of dissolved salt in pore water
t	time
t_D	life expectancy of shrinking particle
T_b	temperature at bond
T_0	equilibrium temperature on flat, stress-free surface
T_s	temperature at stress-free particle surface

ν	flow rate in liquid film
Δ	surface area correction factor
ΔT	temperature difference between stressed and stress-free surfaces
$\Delta\theta$	supercooling correction
$\dot{\epsilon}$	strain rate for ice
μ	viscosity of water
μ'	viscosity of water in thin film
ρ	ice density of snow (excluding pore fluids)
ρ_0	initial ice density of snow
ρ_ℓ	liquid density
ρ_s	solid ice density
σ	stress
σ_b	stress at bond
σ_{bulk}	bulk stress on snow
$\sigma_{\ell g}$	interfacial tension between liquid and gas
σ_{sg}	interfacial tension between solid and gas
$\sigma_{s\ell}$	interfacial tension between solid and liquid
τ	characteristic time

THE COMPRESSION OF WET SNOW

S.C. Colbeck, K.A. Shaw and G. Lemieux

INTRODUCTION

A great deal of information has been generated about the deformation of snow at subfreezing temperatures [e.g., see review by Mellor (1975)], but relatively little is known about the deformation of snow containing liquid water. The Japanese have provided some valuable information on the compression of wet snow (e.g., Kinosita 1963, Ito 1969, Tusima 1973, Wakahama et al. 1974, Wakahama 1975) showing that, with increasing liquid water content, snow is more easily compressed. Yarkin et al. (1972) reported that snow could be strengthened by adding small quantities of salt, a fact that has been used by ski area operators for hardening melting snow surfaces. The potential for the application of knowledge of these and other features of the peculiar properties of wet snow to improve snow removal from highways, control wet snow avalanches, and achieve greater mobility over wet snow covers requires a basic understanding of the material properties of wet snow.

Many studies have been made of phase equilibrium of two- or three-component (water, air and/or ionic impurities) systems. For example, Berry (1959) investigated the dependence of the triple point of water on the size of ice particles. Dorsey (1940) reviewed the effects of pressure, dissolved air, and dissolved ionic impurities on the liquid-solid phase equilibrium temperature. Defay and Prigogine (1951) placed the thermodynamic theory of multi-phase and multi-component systems in a convenient form for application to porous materials just as Dufour and Defay (1963) did for applications to clouds. Using similar methods, Colbeck (1973) developed the relationships describing phase equilibrium in wet snow, showing how the liquid water content and grain size affected the delicate thermodynamics of the material.

Wet snow is a very unusual material in that its response to an applied load can be dominated by small temperature differences between the stressed and stress-free surfaces of the individual particles. These temperature differences arise because the equilibrium temperature at a solid/liquid interface decreases with increasing pressure; hence, the stressed contact surfaces between neighboring particles exist at a temperature which is generally lower than the particles' stress-free pore surfaces. Colbeck (1976) showed that these temperature differences around the surfaces of individual particles account for the rapid deformation of wet snow, including an explanation of the effect of liquid water content on the compressibility of the snow. Colbeck and Parssinen (in press) expanded this model of compressibility to include dissolved ionic impurities and dissolved air but calculated rates of deformation which were generally too large.

In the present study, simultaneous grain growth, the double charged layer at phase boundaries, and an additional mechanism, power law creep, are included in the model. Also, a long series of experiments have been completed and are reported here along with a complete development of the model of the compressibility of wet snow.

EXPERIMENTAL PROCEDURES

Samples of wet snow were prepared by sieving old dry snow and immersing the sieved snow in liquid water for about 24 hours before loading the samples into the experimental apparatus. The mixture was then packed in a test cylinder (see Fig. 1), using a careful procedure in order to achieve a uniform packing of the samples with a density of about 0.48 and an average grain diameter of about 1 mm. These samples were loaded with a "dead weight" whose movement was measured with a displacement transducer (LVDT) in order to calculate the ice density (ice mass per unit volume) throughout the experiment. The most difficult part of the experimental procedure was controlling the temperature of the sample by maintaining the

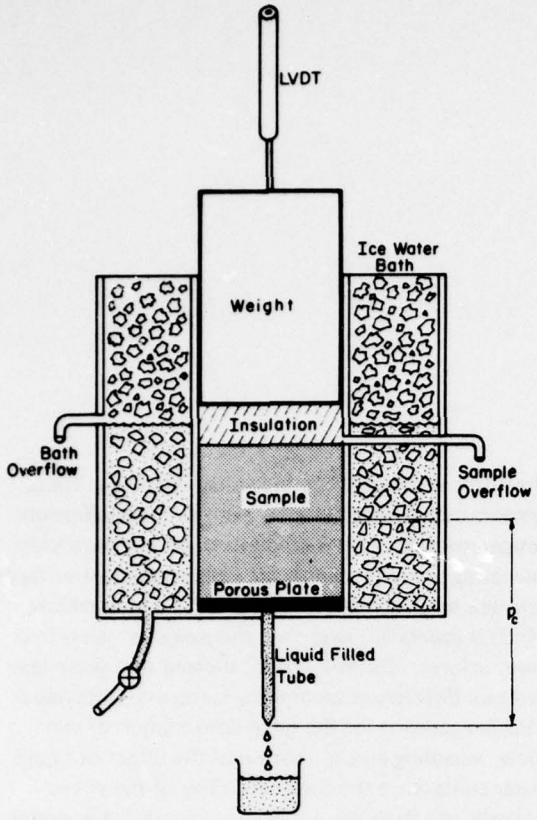

Figure 1. A diagram of the compression apparatus located inside a temperature controlled cabinet.

ice-water bath at the same temperature as the pore water in the sample during the two-week duration of each experiment. In order to achieve proper temperature control, the ice-water bath had to be maintained at the same salinity as the water in the sample and had to be maintained with approximately equal parts of ice and water. This required frequent testing of the sample and bath salinities and additions of salt and/or ice to the bath. Many experiments were rejected because of evidence of melting in the sample or freezing around the weight upon completion of an otherwise successful run.

Two sets of experiments were successfully completed showing the effect of changing the sodium chloride content and the capillary pressure (results are shown later). The capillary pressure was held constant during each experiment by setting the bottom of the water filled tube at a fixed position below the bottom of the sample. Assuming the "liquid path" is continuous, this procedure sets the "tension" in the liquid water in the sample at a value which is constant throughout the experiment. As the compression proceeds, the sample discharges water to maintain the imposed capillary pressure. Unlike other experiments reported in the literature, there was no "saturated layer" at the bottom of these samples and, although the liquid water content varied in all experiments, the parameter of thermodynamic significance (capillary pressure) remained constant during each run.

GRAIN GROWTH

Although the snow grains were immersed in liquid water for 24 hours before being packed into the compression device, grain growth continued throughout the duration of the experiments. After being immersed for 24 hours, the snow grains achieved an average diameter of about 1 mm, and after being stressed and immersed for 2 weeks they reached an average diameter of about 2 mm. In similar experiments, Wakahama (1968) measured the distribution of sizes of snow grains shown in Figure 2. From Figure 2, we calculate the average radius $\bar{r}$ using

$$\bar{r} = \frac{1}{N} \Sigma f_i r_i \qquad (1)$$

and the ratio of particle numbers using conservation of mass, or

$$N\bar{r}^3 = N_0 r_0^3 . \qquad (2)$$

These results are given in Table I for the distributions shown in Figure 2.

Working with bismuth, which has the typical melting temperature-radius relationship, Peppiatt (1975) showed that the number of bismuth particles in the presence of the melt decreases exponentially as a function of time and chose to represent his observations by the relationship

$$N = N_0 \, e^{-t/\tau} . \qquad (3)$$

From eq 2 it follows that we could represent the average particle radius by

$$\bar{r} = r_0 \, e^{t/3\tau} . \qquad (4)$$

However, this suggests that the rate of increase of particle radius increases with time. Wakahama's (1968) data and our data clearly show that the rate of increase of $\bar{r}$ decreases with time; hence, we adopt the expression

$$\bar{r} = r_0 + 1.582 \, (r_\tau - r_0) \, (1 - e^{-t/\tau}) \qquad (5)$$

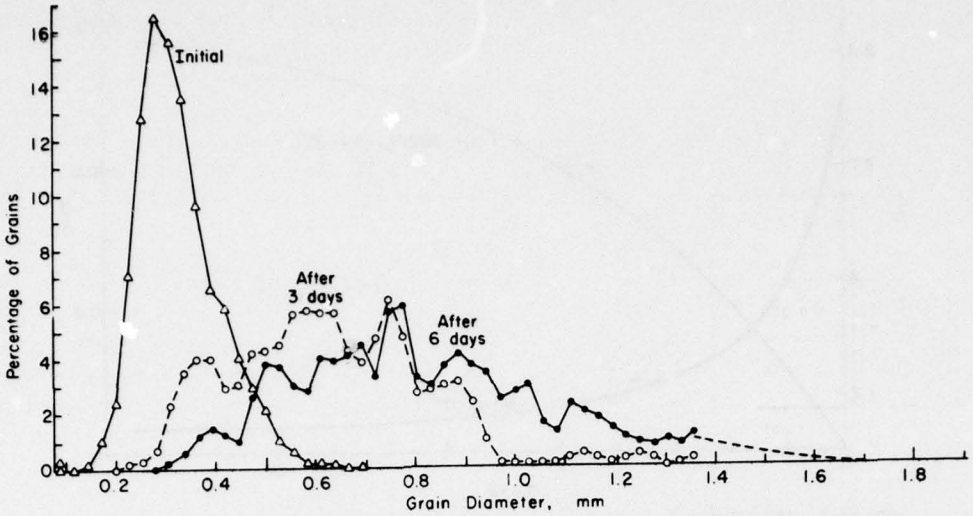

Figure 2. The distribution of sizes of snow grains initially, immersed in water for three days, and immersed in water for six days (after Wakahama 1968). We smoothed the upper end of the distribution for six days.

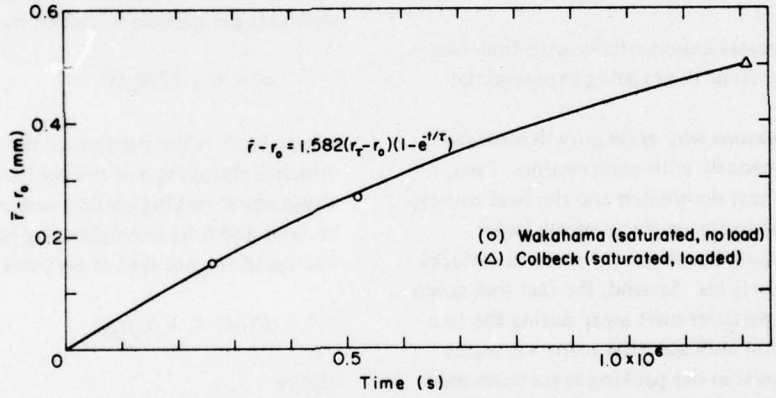

Figure 3. The increase in grain radius shown with time for r_τ = 1 mm and τ = 1,209,600 s.

Table I. Calculations from distributions of Wakahama (1968).

Time (days)	$\Sigma f_i r_i$ *(mm)*	$\bar{r}$ *(mm)*	$\bar{r} - r_0$ *(mm)*	N/N_0
0	32.98	0.165	0	1
3	63.13	0.3155	0.1505	0.143
6	86.12	0.4306	0.2656	0.563

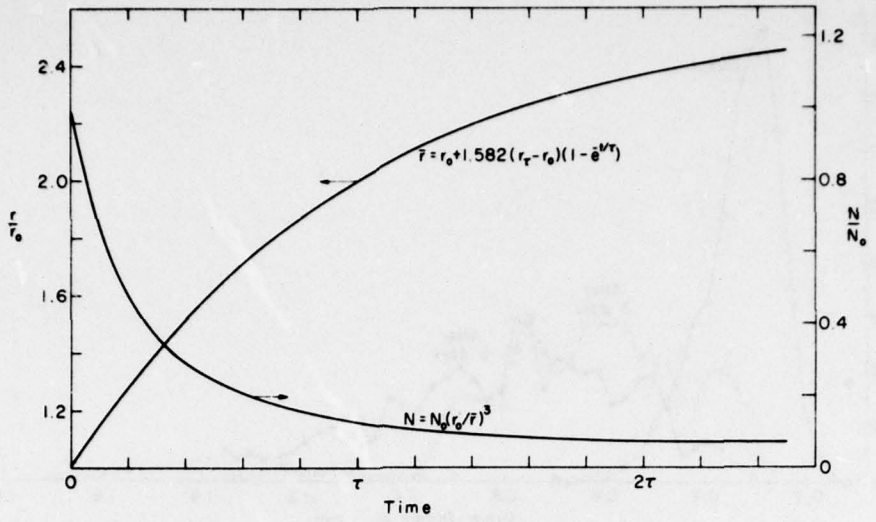

Figure 4. The relative increase in grain radius and decrease in number of particles shown against the characteristic time for $r_\tau = 2r_0$.

which is shown in Figure 3 together with the experimental data. It follows that

$$N = N_0 [1 + 1.582 (r_\tau - r_0)(1 - e^{-t/\tau})/r_0]^{-3} \quad (6)$$

and that dr/dt decreases exponentially with time (see Fig. 4) as shown by all of the existing experimental data.

There are two reasons why grain growth must be considered simultaneously with compression. First, both processes are heat dominated and the heat source, refreezing on the stress-free surfaces of the larger particles, must be shared between the stressed surfaces and the shrinking particles. Second, the fact that seven out of eight of the particles melt away during the two weeks of compression indicates that many vacancies must temporarily exist in the packing as particles melt away from their neighbors. Both Wakahama's (1975) observations and Colbeck's (1973) calculations show that once a particle begins melting it disappears quickly. Thus only a small fraction of the particles is shrinking at any time but, as shown later, these particles reduce the average number of contacts per particle and increase the average stress per contact accordingly.

STRESSED PARTICLE CONTACTS

Visscher and Bolsterli (1972) found an average of 6.4 contacts per sphere in random packings of equal size particles. For simple cubic packings there are 6 contacts per particle, which we use here as the upper limit of the average, although wet snow is a random rather than a systematic packing (the effect of this number on the rate of compression is shown later). Because the shrinking particles are under negligible stress at their contacts, the average number of stressed contacts per particle n is given by

$$n = 6 - 12 N_s/N \quad (7)$$

where N_s/N is the fraction of the particle population which is shrinking and the coefficient (12) arises because one shrinking particle removes 12 contacts (6 of its own and 6 from neighboring particles). The rate of change of the number of particles is given by

$$dN/dt = -N_s/t_D . \quad (8)$$

Hence

$$n = 6 + 12 \frac{t_D}{N} \frac{dN}{dt} \quad (9)$$

or

$$n = 6 - 57 \frac{t_D}{\tau e^{t/\tau}} \frac{r_\tau - r_0}{r_0 + 1.582(r_\tau - r_0)(1 - e^{-t/\tau})} . \quad (10)$$

A typical case (see the parameters listed in Table II) where n increases with time is shown in Figure 5. Over 10^6 s, n increases from about 2 to 5, while the stress at the bonds decreases rapidly. In this example about two-thirds of the particles are stressed initially; hence the average number of stressed bonds per stressed particle

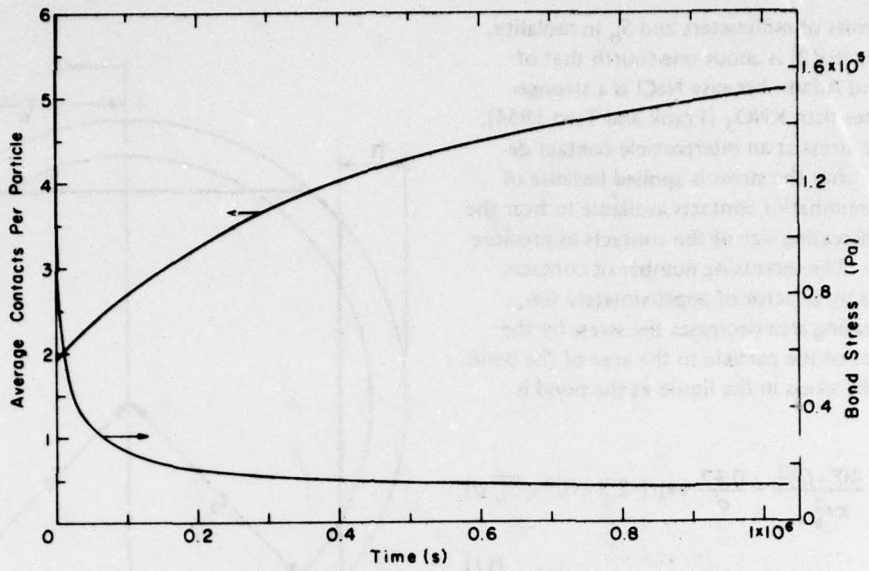

Figure 5. Computed values of the average number of contacts per particle and the fluid stress at a bond shown against time for parameters shown in Table II.

Table II. Parameters for various figures.

Figure	σ_{bulk} (Pa)	S_s	r_0 (mm)	r_τ (mm)	τ (s)	t_D (s)	p_c
5	11,790	0.0007	0.5	1	1,209,000	86,400	0
8	11,790	0.0007	0.5	1	1,209,000	86,400	0
9	11,790	0.0007	0.5	1	1,209,000	86,400	0
10	10^6	0.0007	0.5	1	1,209,000	86,400	0
11	4,790	0.0007	0.5	1	1,209,000	86,400	4 values
12	11,790	3 values	0.5	1	1,209,000	86,400	0
13	11,790	4 values	0.5	1	1,209,000	86,400	0
14	4,790	0.0007	3 values	4 values	1,209,000	86,400	0
15	4,790	0.0007	0.5	1	1,209,000	3 values	0
16	4,790	0.0007	0.5	3 values	1,209,000	86,400	8,923 Pa
17	4,790	0.0007	0.5	1	1,209,000	86,400	0
18	4,790	0.0007	0.5	1	1,209,000	86,400	0
19	4,790	varies	2 values	2 values	1,209,000	86,400	varies

is about 3 initially. Thus there are enough stressed contacts to make the particles stable geometrically at all times.

FLUID PRESSURE

As the densification proceeds, the thickness of the liquid film between the particles approaches 10^{-5} mm; hence we must consider the electrostatic forces which arise due to the double charged layers at each solid-liquid boundary (see cover photo). It is generally agreed that these forces decay exponentially with separation (Israelachvili and Ninham 1977, Aveyard and Haydon 1973, p. 43, Adamson 1967, p. 218) and increase with decreasing salinity (Israelachvili and Adams 1976). While the van der Waal forces at this separation are small, the repulsive forces between the double layers are significant and counteract the applied load, especially at low salinities. From the experimental results of Israelachvili and Adams (1976), who used KNO_3 solution, we deduce that the repulsive force per unit area between two flat surfaces separated by a NaCl solution is

$$\frac{0.42}{d} \exp\left(-2.3\times10^6 \sqrt{S_b}\, d\right) \quad \text{(units of Pascals)}$$

where d is in units of millimeters and S_b in molality. The coefficient (0.42) is about one-fourth that of Israelachvili and Adams because NaCl is a stronger structure former than KNO_3 (Frank and Tsao 1954).

The average stress at an interparticle contact decreases rapidly after the stress is applied because of the increasing number of contacts available to bear the load and the increasing size of the contacts as pressure melting occurs. The increasing number of contacts decreases stress by a factor of approximately $6/n$, while the increasing area decreases the stress by the ratio of the area of the particle to the area of the bond. Accordingly, the stress in the liquid at the bond is given by

$$\sigma_b = \sigma_{bulk} \frac{6}{n} \frac{4(\bar{r}-D)^2}{\pi r_b^2} - \frac{0.42}{d} \exp(-2.3\times10^6 \sqrt{S_b}\, d). \quad (11)$$

PACKING GEOMETRY

The depth of the melted cap D and the radius of the bond can be calculated at each stage of the deformation from the conservation of the total ice mass in the sample, or (see Fig. 6)

$$8r_0^3 N_0 = 8r_p^3 N - n N h (h^2 + 3r_b^2) \quad (12)$$

where

$$h = r_p - (r_p^2 - r_b^2)^{1/2} . \quad (13)$$

Given these values we can calculate the ice density of the sample from

$$\rho = \rho_0 \left(\frac{\bar{r}}{\bar{r}-D}\right)^{n/2} \quad (14)$$

which is an exact expression for simple cubic packings where n is an integer. The computations are made iteratively by calculating the rate of increase of D at each step and then updating the geometrical variables.

TEMPERATURE DISTRIBUTION AND HEAT FLOW

The rate of increase of D is given by the heat flow from the stress-free to the stressed surfaces minus a correction for the heat diverted to the shrinking particles. Accordingly,

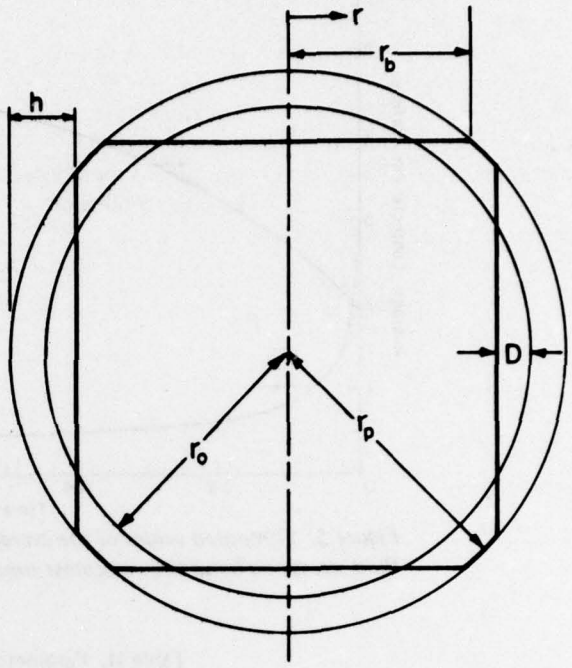

Figure 6. The cross-sectional view of a typical particle symmetrically developing four melt caps. The smaller circle represents the initial particle radius and the larger circle represents the increased particle radius due to the refreezing on the stress-free surfaces.

$$\frac{dD}{dt} = \frac{k_i}{L\rho_s}\left(\frac{\Delta}{r_p}\right)\frac{2+n}{2\pi}(\Delta T) - \frac{75.9}{n^2+2n}\left(\frac{\bar{r}}{r_b}\right)^2 \frac{r_\tau - r_0}{\tau} e^{-t/\tau} \quad (15)$$

where

$$\Delta = \begin{cases} 1 & \text{if } \dfrac{2r_p^2 - 6r_p h}{3r_b^2} > 1 \\ \dfrac{2r_p^2 - 6r_p h}{3r_b^2} & \text{if } \dfrac{2r_p^2 - 6r_p h}{3r_b^2} < 1 \end{cases} \quad (16)$$

and ΔT is the temperature difference between the stressed and stress-free surfaces. The first term in eq 15 represents the heat flow due to the temperature difference ΔT, whereas the second term reduces the heat flow to account for the fact that simultaneous particle growth diverts some heat away from the only source, refreezing on the stress-free surfaces of the ice particles. The first term takes the varying number of

stress contacts per particle n into account because the average path length for heat flow decreases with increasing n. Also, the ratio of the surface areas acting as heat sources and heat sinks is accounted for by Δ. The second term is derived from a total heat balance.

The temperature difference ΔT is equal to the phase equilibrium temperature of the stress-free surface minus the phase equilibrium temperature of the stressed surface minus a small correction for supercooling on the stress-free surface,

$$\Delta\theta = -0.0673\left(\frac{\Delta r_b T_s}{2r_p^2}\right)^{3/4}. \qquad (17)$$

There are two regimes of liquid saturation, *pendular* and *funicular*, which must be considered separately. In the pendular regime of lower saturation where the air phases exist in continuous paths throughout the pore space, the phase equilibrium at the stress-free surfaces is (Colbeck 1973):

$$T_s = -\frac{T_0}{\rho_\ell L} p_c - \frac{2T_0}{\rho_s L}\frac{\sigma_{sg}}{r_p} - \frac{RT_0^2}{L} / S_s \qquad (18)$$

where the first term arises due to capillary pressure, the second due to the size of the ice particles, and the third due to dissolved, ionic impurities. At higher liquid saturations where the liquid phase exists in continuous paths throughout the pore space, the phase equilibrium temperature at the stress-free surfaces is

$$T_s = \frac{2T_0}{L}\left(\frac{1}{\rho_\ell} - \frac{1}{\rho_s}\right)\frac{\sigma_{\ell g}}{r_a} - \frac{2T_0}{L\rho_s}\frac{\sigma_{s\ell}}{r_p} - \frac{RT_0^2}{L} / S_s \qquad (19)$$

where the first term arises due to the radius of the trapped air bubbles. The temperature of the stressed surfaces at the inter-particle contacts (see Fig. 7) is given by

$$T_b = \frac{T_0}{L}\left(\frac{1}{\rho_\ell} - \frac{1}{\rho_s}\right)\sigma_b + 0.0024\left(\frac{C_s - C_b}{C_s}\right) - \frac{RT_0^2}{L} / S_b \qquad (20)$$

where the first term is the temperature decrease due to the stress exerted on the solid by the liquid (the double layer forces cancel at each interface; hence T_b is determined by fluid pressure only), the second term is the temperature increase due to the relative absence of dissolved air in the melt, and the third term is the temperature decrease due to the presence of dissolved ionic impurities. Note that no pressure melting would occur if water were an ordinary substance and contracted upon freezing because the first term would then be positive and the solid-liquid equilibrium temperature would increase with increasing stress.

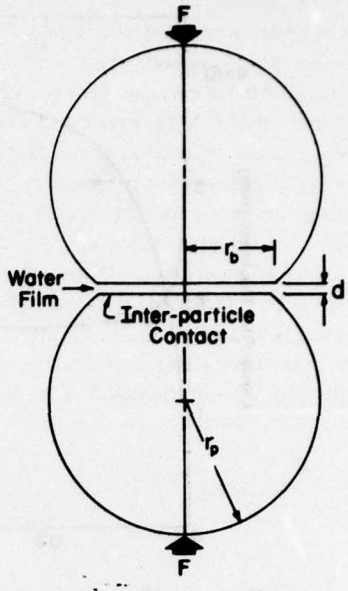

Figure 7. Two particles pushed together melt at the stressed surfaces. The melt water is removed in a thin film and refreezing takes place on the stress-free, rounded surfaces.

FLUID AND IMPURITY FLOWS

The concentrations of dissolved air C_b and ionic impurities S_b in the melt water being flushed through the thin film between the particles is of critical importance to the rate of compression of wet snow. Drake and Shreve (1973) showed that wires moving through ice by regelation behave similarly, although the source of the dissolved impurities, diffusion from the pore water into the very thin film of liquid between the particles (see Fig. 8), would seem to be very slow because of its small size. Despite this small size, the particle path for diffusion is also very small and the concentration gradients are fairly large.

The melt water moves radially outward through the liquid film at a rate given by (Moore 1965)

$$v = \frac{Fd^2 r}{3\pi\mu r_b^4}. \qquad (21)$$

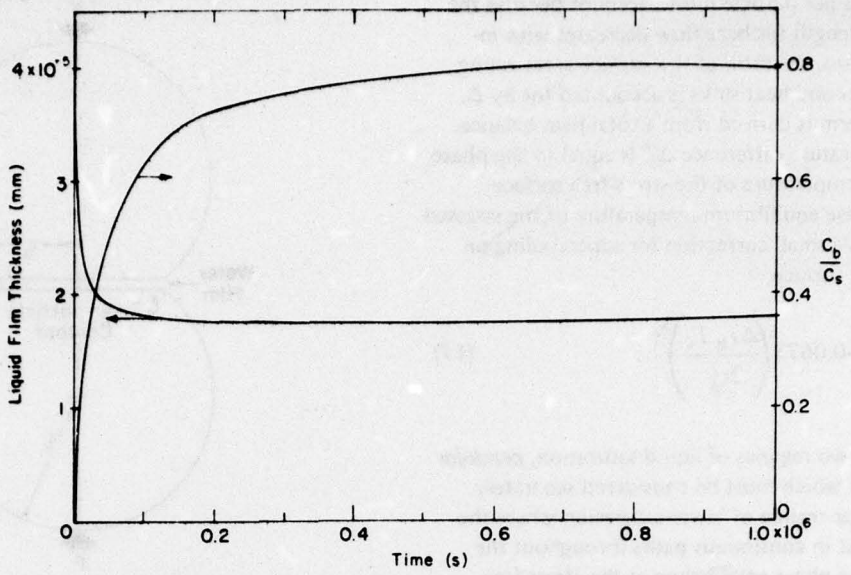

Figure 8. The computed size of the liquid film between the particles and the fraction of dissolved impurities reaching the bond shown against time for typical conditions.

Continuity requires

$$v = \frac{r}{d}\frac{\rho_s}{\rho_\ell}\frac{dD}{dt}. \tag{22}$$

Hence the film thickness is

$$d = \left[\frac{3\mu(\rho_s/\rho_\ell)r_b^2\,(dD/dt)}{\sigma_b}\right]^{1/3}. \tag{23}$$

Here we assume distinct phase boundaries and a film of homogeneous liquid whose flow is not affected by charge separation. Some modifications to these assumptions are suggested later.

Assuming a quasi-steady balance between the movement of the impurities with the melt water and the diffusion of the impurities against the flow of the melt water,

$$vC + D_i\frac{dC}{dr} = 0 \tag{24}$$

or the distribution of the impurities is given by

$$C_b = C_s \exp\left(-\frac{1}{D_i}\frac{\rho_s}{\rho_\ell}\frac{dD}{dt}\int_0^{r_b}\frac{r}{d}\,dr\right) \tag{25}$$

where C_b is the concentration at the center of the contact. Assuming that the contact surfaces are flat [$d \neq f(r)$], we can simplify eq 25, but there is a complicated feedback involving the impurity concentration, the double charged layer, the temperature difference, the rate of melting, the melt water discharge rate and, again, the impurity concentration. This feedback loop demonstrates the delicate nature of the pressure melting mechanism.

Another mechanism, nonlinear viscous creep of the ice in the region of the stressed contacts, is also considered. Wilkinson and Ashby (1975) show that for a material with a power law relationship between stress and strain rate, or

$$\dot{\epsilon} = A\,\sigma^m \tag{26}$$

the rate of densification ($d\rho/dt$) due to the creep of the material at the contact is

$$\frac{d\rho}{dt} = \frac{3}{4}A\rho_0\frac{r_b}{\bar{r}}\left(\frac{3}{2}\frac{A_f}{\pi r_b^2}\frac{\sigma_{bulk}}{m}\right)^m.$$

Here A_f is $4\bar{r}^2$ for a simple cubic packing. We take m as three and, from the results of Colbeck and Evans (1973), we take A equal to 1.28×10^{-23} ($Pa^{-m}\ s^{-1}$) for polycrystalline ice in thermal equilibrium with the melt. For a typical case, calculated values of the rate of densification are shown for both the total and nonlinear viscous deformation mechanisms in Figure 9. Clearly regelation is the dominant mechanism in this example, but because the rate of densification due to

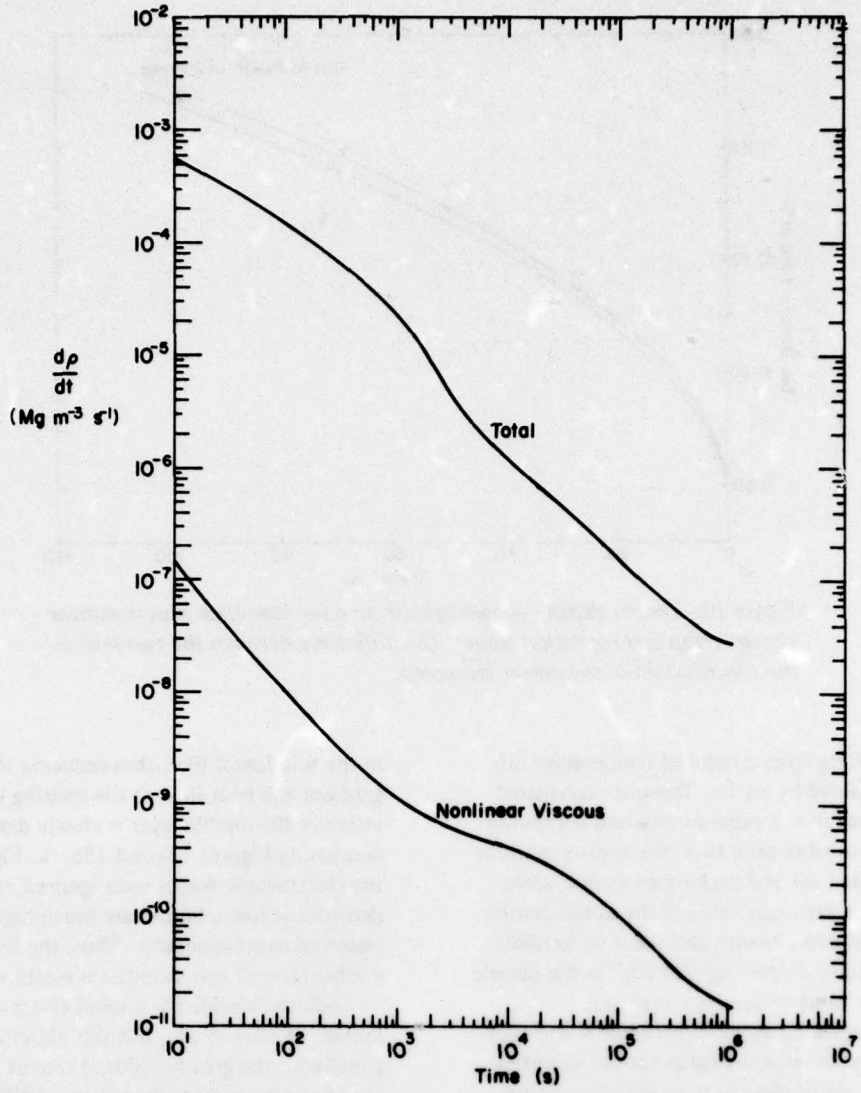

Figure 9. The computed rates of densification shown for the total and the nonlinear viscous deformations.

power law creep increases as a high power of stress, whereas the temperature depression causing regelation increases as only the first power of stress, the nonlinear mechanism is relatively more important at higher stresses.

The ice density is shown as a function of time in Figure 10 for an applied stress of 10^6 Pa. This shows that even at stresses as large as the overburden pressure at the firn-ice transition in a temperate glacier, regelation is still the dominant mechanism. This conclusion is reinforced by observations [e.g., Vallon et al. (1976)] which have shown a correlation between the rate of firnification and the liquid water content of the snow. This correlation can be readily explained in terms of the regelation described here.

RESULTS

As already shown by the results given in Figures 5, 8, 9 and 10, a model has been constructed using the concepts described in the previous section. The expermental results at various liquid water contents are shown together with computed curves in Figures 11a and 11b. Both sets of curves clearly show the decreased rate of densification at lower liquid contents (higher capillary

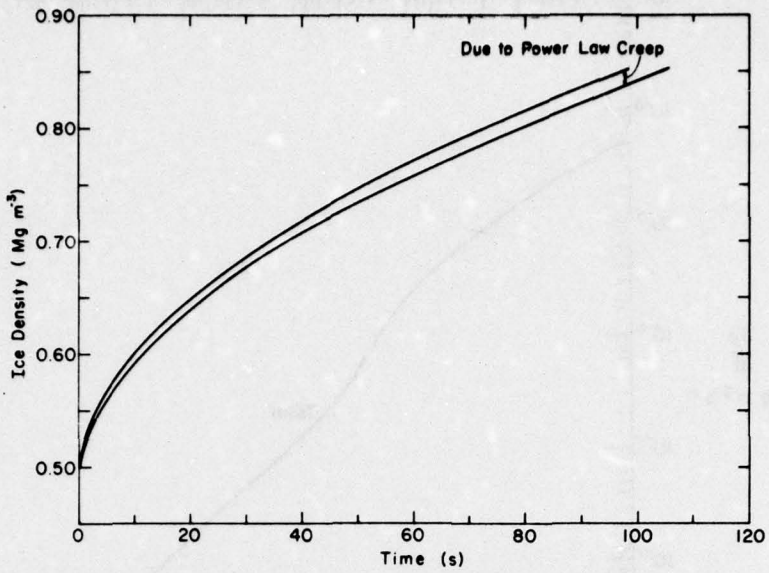

Figure 10. The ice density shown against time for regelation plus nonlinear viscous creep and regelation alone. The difference between the two lines is the contribution of the power law creep.

pressures) resulting from a reduced temperature difference as explained by eq 18. There are consistent differences between the experimental and computed results which probably arise from the approximations made about heat flow and packing geometry, some uncertainty over the exact value of the initial density in the individual experiments, and some uncertainty over the continuity of the "liquid path" in the sample with the largest value of capillary pressure.

Similarly, Figure 12 shows experimental and computed results for snow saturated at various salinities. The decreased rate of densification with increasing salinity is apparent in both sets of curves, although there are differences between the computed and measured results. Given the severe experimental limitations inherent in long-term loading of samples of wet snow, we do not know whether the major problems are with the fine points of the experiments or the model. Because of the severe difficulties of working with this material and the variety of parameters which are involved, the model is very useful to help understand the physical processes, to identify important parameters, and to make quick estimates of the compressibility under widely varying conditions.

Figure 13a shows the wide range of responses computed for different salinities. The largest change occurs as salinity decreases to 10^{-3} where the double charged layer begins to dominate other processes. At lower salinities the double charged layer decreases the stress in the thin liquid film, thus reducing the temperature gradient and heat flow to the melting surfaces. This effect of the double layer is clearly demonstrated by comparing Figures 13a and 13b. In Figure 13b where the electrostatic forces were ignored, the computed densities at low salinities are much higher than those observed experimentally. Thus, the importance of the double layer at low salinities is established.

Sodium chloride has a small effect on the rate of growth of snow grains, but this effect is small compared with the greatly reduced rate of growth at low liquid water contents (Wakahama 1975). No doubt the imposed load also changes the rate of grain growth; hence it is necessary to investigate these matters here. Figure 14 shows the computed increase in ice density with time for four situations with different grain radii. For a constant grain radius of 0.5 mm, the largest rate of densification occurs because there is no heat diversion to growing particles and because the heat flow path length is smallest for smaller particles. At a constant radius of 1 mm, the computed rate of densification is reduced markedly because of the larger path length for heat flow. The measured increase in ice density with time for a particle size of 3 to 4 mm shown in Figure 14 confirms this idea about the heat flow path length. It is rather suprising that there is little difference between the densification of particles of a constant 1-mm radius and those which grow from 0.5 to 1 mm during the densification. The densification of particles which

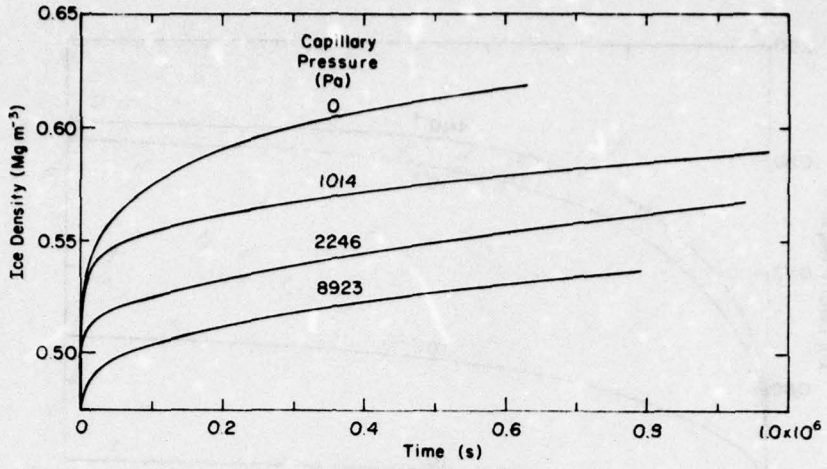

a. Experimental results.

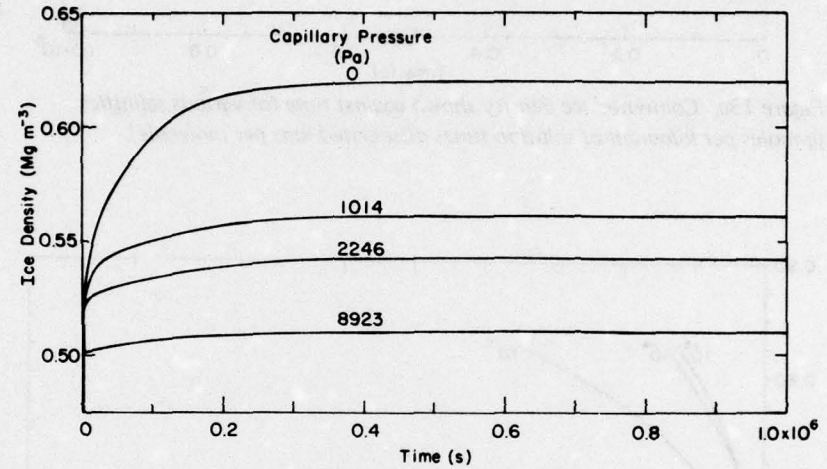

b. Computed results.

Figure 11. Ice density shown against time for various capillary pressures for both experimental (a) and computed (b) results.

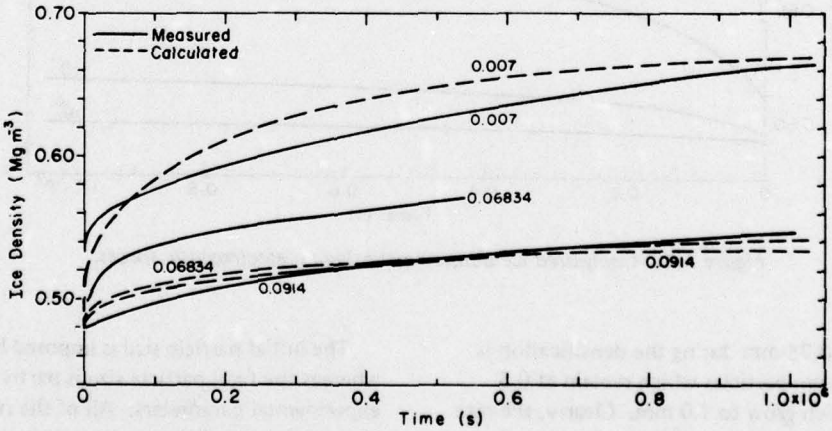

Figure 12. Ice density shown against time for various sodium chloride contents (g-moles NaCl per kilogram of solution times dissociated ions per molecule) for experimental and computed results.

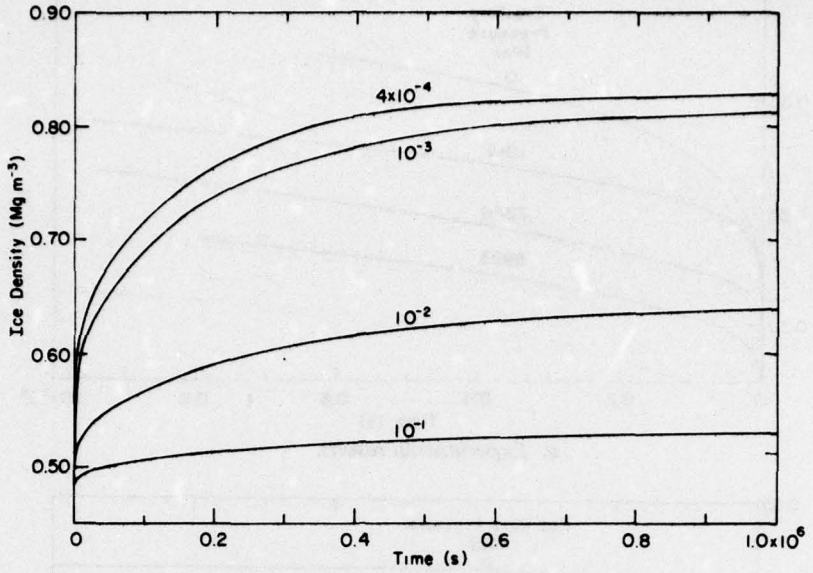

Figure 13a. Computed ice density shown against time for various salinities (g-moles per kilogram of solution times dissociated ions per molecule).

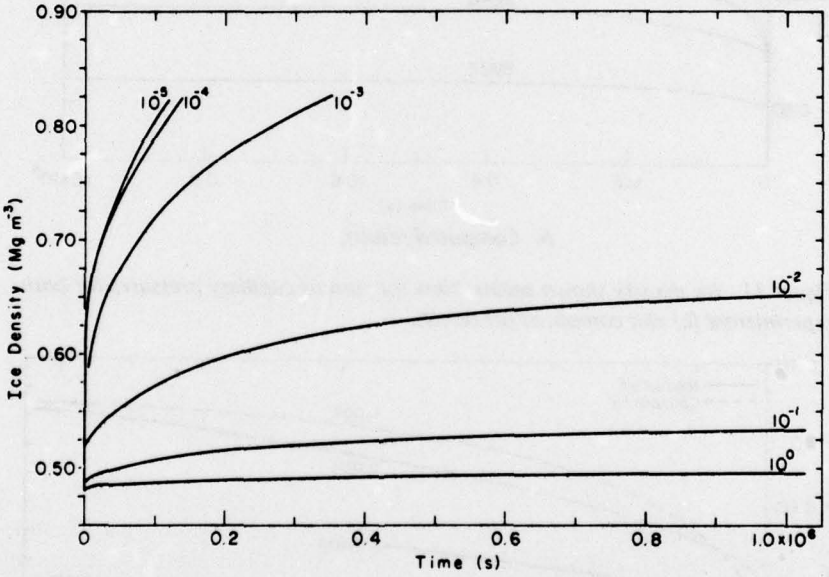

Figure 13b. Computed ice density assuming no electrostatic forces.

grow from 0.5 to 0.75 mm during the densification is intermediate between particles which remain at 0.5 mm and those which grow to 1.0 mm. Clearly, the rate of particle growth has a major effect on the rate of densification in saturated snow and the characteristics of the growth must be well known in order to quantify the compression of wet snow.

The initial particle size is imposed by the situation, whereas the final particle size is partly the result of the experimental parameters. All of the required information can be supplied from knowledge of the conditions under which the deformation takes place and observations of particle growth under similar conditions. The average life expectancy of a shrinking particle t_D can

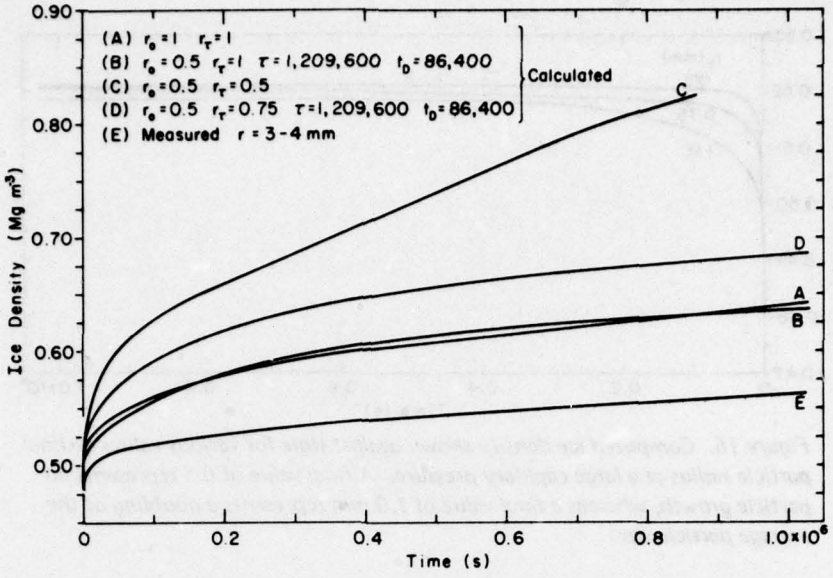

Figure 14. Four examples of computed ice density are shown against time for various particle radii and rates of particle growth. One experimental result is shown for large ice chips of 3 to 4-mm diameter.

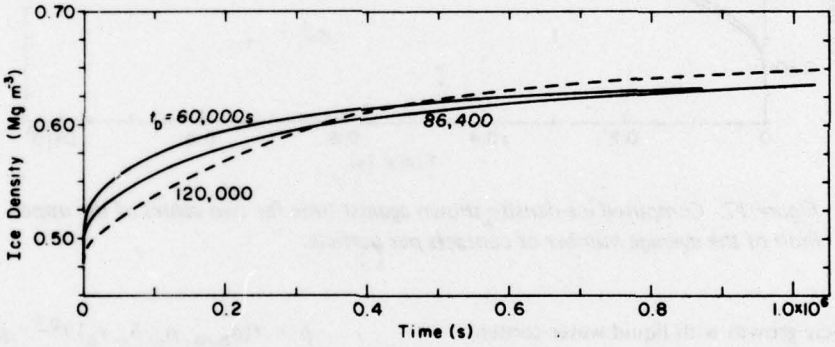

Figure 15. Computed ice density shown against time for various life expectancies for an average shrinking particle.

be determined using techniques like Wakahama's (1975) time-lapse photography or Colbeck's (1973) calculations of particle capture. Here we have chosen a value of 1 day (86,400 s) which is in the range of the life expectancies observed and calculated. As shown in Figure 15, the computed rate of densification is not too sensitive to this parameter; hence it is not necessary to adjust the life expectancy to accommodate changes in the other parameters in order to use this model.

At large capillary pressures or large salinities, the effect of simultaneous particle growth is greatly reduced because of the altered temperature field. Apparently, simultaneous heat diversion to growing particles is not of much consequence when the temperature of the stress-free particle surfaces is reduced by low liquid contents or large concentrations of impurities in the pore water. Figure 16 shows the effect of changing the particle radius after growth r_τ for an initial particle radius of 0.5 mm at a capillary pressure of 8923 Pa. It is clear from Figures 14 and 16 that simultaneous particle growth has a greatly reduced effect on densification at large capillary pressures; hence the varying rate of particle growth with liquid water content is not the important parameter we might have supposed. This greatly simplifies the use of this model, since for most purposes we can ignore the

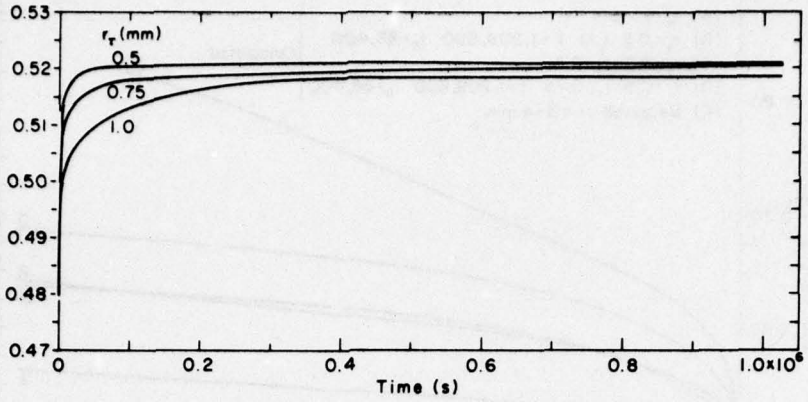

Figure 16. Computed ice density shown against time for various values of final particle radius at a large capillary pressure. A final value of 0.5 represents no particle growth, whereas a final value of 1.0 mm represents a doubling of the average particle size.

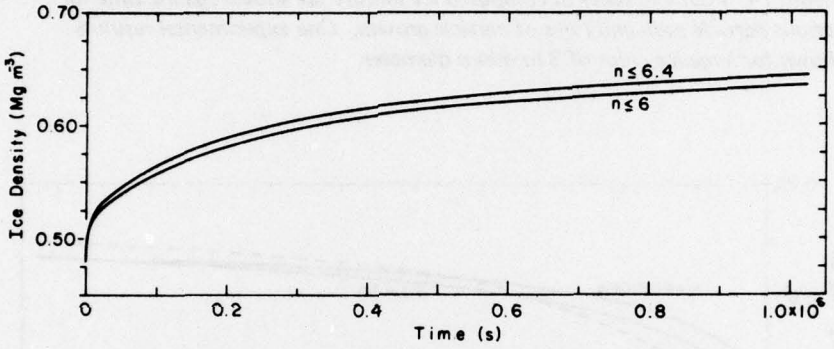

Figure 17. Computed ice density shown against time for two values of the upper limit of the average number of contacts per particle.

variation of particle growth with liquid water content and salinity.

We used a simple cubic packing for assistance in conceptualizing at several steps in previous sections; for example, in the derivation of eq 7, we used a maximum of 6 contacts per particle rather than the average of 6.4 calculated by Visscher and Bolsterli (1972). We are now in a position to show that this assumption has a small effect on the values computed using this model. Figure 17 shows the result of changing the average number of contacts per particle from 6 to 6.4 and, as with the various values for t_D shown in Figure 15, there is very little error resulting from the use of this approximation.

The results shown in Figure 9 suggest that the rate of density increase is proportional to time to the power negative 0.8. Therefore we may express the density of wet snow as

$$\rho = f(\sigma_{bulk}, p_c, S_s, r_0)\, t^{0.2} + \rho_0 . \qquad (28)$$

This expression is compared with the computed and measured values of density and time for a particular case in Figure 18, where it can be seen that, as long as the parameters can be included properly, this simple expression could be a highly accurate substitute for the computations. For many purposes, it may be better to work with this expression, adjusting the coefficient as required to account for the particular parameter under consideration.

Just as St. Lawrence (unpublished) showed for low density snow at subfreezing temperatures, it is possible to describe the deformation of high density, wet snow by physical considerations on the scale of individual particles. The most significant difference between subfreezing and wet snow is the regelation mechanism described here. For example, dry snow and saturated

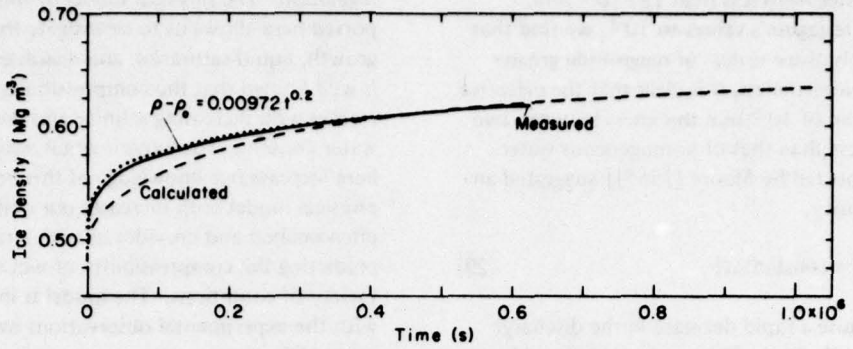

Figure 18. Computed and measured ice densities shown against time and compared with an algebraic expression.

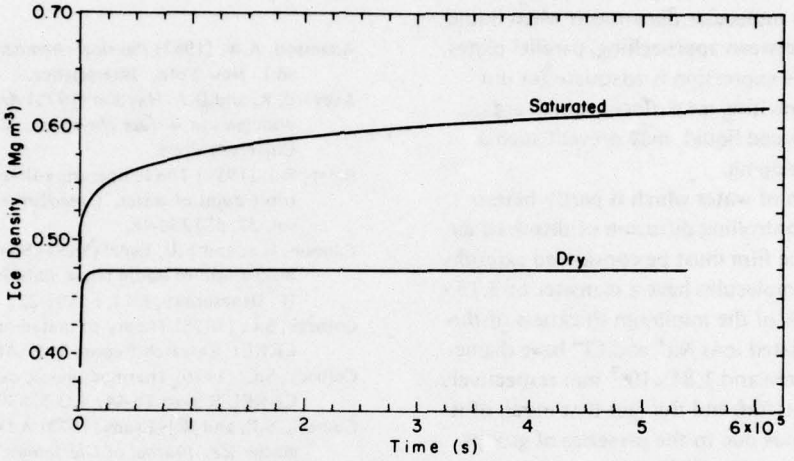

Figure 19. Measured ice density shown against time for dry snow at –2°C and saturated snow.

snow compressed at the same stress are shown in Figure 19. Upon application of the load, the dry snow quickly compresses up to a density of 0.474, the approximate density at which the wet snow samples were packed. Above that density the deformation of dry snow is limited by the slow processes of creep at the stressed contacts and other sintering mechanisms described by Hobbs (1965).

Sintering in the presence of the liquid phase in metals is dominated by the "solution – deposition" mechanism (Kingery 1958, Courtney 1977) where smaller particles disappear because of their greater solubility. Like pressure melting in wet snow, solution-deposition is also sensitive to simultaneous particle growth (Cannon and Lenel 1953). Also, sintering in metals is enhanced by deformation at the stressed contacts (Murray et al. 1958, Wilkinson and Ashby 1975).

THE LIQUID FILM

While the concept of compaction by pressure melting is well established for wet snow, several limitations of the model are important. The simplified treatment of heat flow and reference to a simple cubic packing have already been noted, but the most serious limitations of this model may be the assumptions made about the very thin liquid film between the stressed particles. There are several reasons for concern. First, Figure 8 shows a typical thickness of this film of only 10^{-5} mm. Although Moore (1965) states that no molecular influence can exist at 1.27×10^{-5} mm from the surface in films of mineral or vegetable oil, and Buckley [as reported by Dorsey (1940)] found no stationary film of oil at thicknesses as large as 3×10^{-5} mm, Derjaguin [as reported by Dorsey (1940)] found some elastic

"rigidity" in water films less than 15×10^{-5} mm. Extrapolating Derjaguin's values to 10^{-5}, we find that viscosity is nearly three orders of magnitude greater than rigidity. Nevertheless, it is clear that the effective viscosity of a film of 10^{-5} mm thickness between two ice surfaces is less than that of homogeneous water. Terzaghi [as reported by Moore (1965)] suggested an equivalent viscosity,

$$\mu' = \mu(1 + \text{constant}/d) \qquad (29)$$

which would cause a rapid decrease in the discharge with decreasing film size. This type of relationship would be included in the current model if the appropriate value could be attached to the constant. Needs [as reported by Moore (1965)] showed that d has a lower limit close to molecular dimensions when liquid is displaced from between approaching, parallel plates. However, Terzaghi's expression is adequate for our purposes since the melting ice surfaces, which are sources of the displaced liquid, may prevent such a thin film from developing.

Given a thin film of water which is partly heterogeneous, the rate controlling diffusion of dissolved air and ions through the film must be considered carefully. Dissolved nitrogen molecules have a diameter of 3.15×10^{-7} mm or over 3% of the minimum thickness of the liquid film. Dissociated ions Na^+ and Cl^- have diameters of 0.97×10^{-7} mm and 1.81×10^{-7} mm respectively. Given the size of the film and the fact that much of it may be heterogeneous due to the presence of groups of molecules, it follows that diffusion may occur more slowly in these thin films than in homogeneous water. If so, the diffusion of impurities through the film would be less than calculated, and the temperature gradient and heat flow would be reduced, thus reducing the rate of melting and the liquid flow through the film. However reducing the flow would increase the diffusion of impurities; hence both the increased viscosity and reduced diffusivity have limited effects because of this stable feedback mechanism in the regelation process.

Preferential incorporation of cations or anions with the freezing liquid on the stress-free surfaces can cause charge separation in the pore water (Cross 1972). This may or may not enhance the perferential diffusion of ions into the thin film, but the double layer already described is clearly important. The treatment of that double layer could be improved if there were direct evidence of its strength for an ice surface and a sodium chloride solution.

CONCLUSIONS

Wet snow is a very unusual material which, at intermediate to high densities, deforms predominantly by regelation. The physical model of this process reported here allows us to investigate the effects of grain growth, liquid saturation and dissolved impurities. It is well known that the compressibility of wet snow decreases with increasing salinity and decreasing liquid water content. The experimental observations reported here increase our knowledge of this behavior and the physical model both increases our understanding of the phenomenon and provides us with a reliable method of predicting the compressibility of wet snow under a variety of conditions. The model is in fair agreement with the experimental observations over a wide range of conditions.

LITERATURE CITED

Adamson, A.W. (1967) *Physical chemistry of surfaces* (2nd ed.). New York: Interscience.

Aveyard, R. and D.A. Haydon (1973) *An introduction to the principles of surface chemistry*. Cambridge: Cambridge University Press.

Berry, R.J. (1959) The temperature-time dependence of the triple point of water. *Canadian Journal of Physics*, vol. 37, p. 1230-48.

Cannon, H.S. and F.U. Lenel (1953) Some observations on the mechanism of liquid phase sintering. *Plansee Proceedings* (F. Benesousky, Ed.), p. 106-22.

Colbeck, S.C. (1973) Theory of metamorphism of wet snow. CRREL Research Report 313. AD 772692.

Colbeck, S.C. (1976) Thermodynamic deformation of wet snow. CRREL Report 76-44. AO 33830.

Colbeck, S.C. and R.J. Evans (1973) A flow law for temperate glacier ice. *Journal of Glaciology*, vol. 12, no. 64, p. 71-86.

Colbeck, S.C. and N. Parssinen (in press) Regelation and the deformation of wet snow. *Journal of Glaciology*.

Courtney, T.H. (1977) A reanalysis of the kinetics of neck growth during liquid phase sintering. *Metallurgical Transactions A*, vol. 8A, p. 671-77.

Cross, G.W. (1972) Solute interference effects in freezing potentials of dilute electrolytes. *Water Structure at the Water-Polymer Interface* (H.H.G. Jellinek, Ed.), New York: Plenum Press.

Defay, R. and I. Prigogine (1951) *Tension superficielle et adsorption*. Liége: Editions Desoer.

Dorsey, N.E. (1940) *Properties of ordinary water-substance*. New York: Reinhold.

Drake, L.D. and R.L. Shreve (1973) Pressure melting and regelation of ice by round wires. *Proceedings, Royal Society of London*, vol. A332, no. 1588, p. 51-83.

Dufour, L. and R. Defay (1963) *Thermodynamics of clouds*. New York: Academic Press.

Frank, H.S. and M.-S. Tsao (1954) Solutions of electrolytes. *Annual Reviews of Physical Chemistry* (G.K. Roblefson and R.E. Powell, Ed.), *Annual Reviews*, Stanford, vol. 5, p. 43-70.

Hobbs, P.V. (1965) The effect of time on the physical properties of deposited snow. *Journal of Geophysical Research*, vol. 70, no. 16, p. 3903-07.

Israelachvili, J.N. and G.E. Adams (1976) Direct measurement of long range forces between two mica surfaces in aqueous KNO_3 solutions. *Nature*, vol. 262, no. 5571, p. 774-76.

Israelachvili, J.N. and B.W. Ninham (1977) Intermolecular forces – the long and short of it. *Journal of Colloid and Interface Science*, vol. 58, no. 1, p. 14-25.

Ito, H. (1969) Unconfined compression test of wet snow. *Japanese Journal of Snow and Ice*, vol. 31, no. 9, p. 7-18.

Kingery, W.D. (1958) Sintering in the presence of a liquid phase. *Ceramic Fabrication Processes* (W.D. Kingery, Ed.), Cambridge: MIT Press, p. 131-43.

Kinosita, S. (1963) Compression of snow immersed in water of 0°C. I. *Low Temperature Science*, ser. A, vol. 21, p. 13-22.

Mellor, M. (1975) A review of basic snow mechanics. In *Snow Mechanics Symposium (Proceedings of Grindelwald Symposium, April 1974)*. International Association of Scientific Hydrology Publ. No. 114, p. 251-91.

Moore, D.F. (1965) A review of squeeze films. *Wear*, vol. 8, p. 245-63.

Murray, P., D.T. Livey and J. Williams (1958) The hot pressing of ceramics. *Ceramic Fabrication Processes* (W.D. Kingery, Ed.), Cambridge: MIT Press, p. 147-71.

Peppiatt, S.J. (1975) The melting of small particles. II Bismuth. *Proceedings, Royal Society of London*, vol. A345, p. 401-12.

St. Lawrence, W.F. (unpublished) A structural theory for the deformation of snow. Ph.D. Thesis. Dept. of Civil Engineering, Montana State University.

Tusima, K. (1973) Tests of the repeated loadings on snow. *Low Temperature Science*, ser. A, vol. 31, p. 57-68.

Vallon, M., J.R. Petit and B. Fabre (1976) Study of an ice core to the bedrock in the accumulation zone of an alpine glacier. *Journal of Glaciology*, vol. 17, no. 75, p. 13-28.

Visscher, W.M. and M. Bolsterli (1972) Random packing of equal and unequal spheres in two and three dimensions. *Nature*, vol. 239, p. 504-07.

Wakahama, G. (1968) The metamorphism of wet snow. Commission of Snow and Ice. IUGG, IAHS, *General Assembly of Bern*, Sept-Oct 1967, p. 370-79.

Wakahama, G. (1975) The role of melt-water in densification processes of snow and firn. *Snow-Mechanics Symposium (Proceedings of the Grindelwald Symposium)*, IAHS Publ. No. 114, p. 66-72.

Wakahama, G., D. Kuroiwa and C.S. Benson (1974) Field studies on the transformation processes of snow into glacier ice in the accumulation area of McCall Glacier, Alaska. *Low Temperature Science*, ser. A, vol. 32, p. 143-59.

Wilkinson, D.S. and M.F. Ashby (1975) Pressure sintering and power law creep. *Acta Metallurgica*, vol. 23, no. 11, p. 1277-85.

Yarkin, I.G., I.A. Tyutyunov and A.V. Sadovskii (1972) Physiochemical method of strengthening snow. *Osnovaniya Fundamenty i Mekhanika Gruntov*, no. 4, p. 21-22.

In accordance with letter from DAEN-RDC, DAEN-ASI dated 22 July 1977, Subject: Facsimile Catalog Cards for Laboratory Technical Publications, a facsimile catalog card in Library of Congress MARC format is reproduced below.

GB
2405
.C6
Report
78-10

Colbeck, S.C.
The compression of wet snow / by S.C. Colbeck, K.A. Shaw and G. Lemieux. Hanover, N.H.: U.S. Cold Regions Research and Engineering Laboratory, 1978.
vi, 23 p: ill.; 27 cm. (CRREL Report; 78-10)
Prepared for Directorate of Facilities Engineering - Office, Chief of Engineers under DA Project No. 4A161102AT24
Literature cited: p. 16.
1. Compressibility. 2. Liquids. 3. Salinity. 4. Viscous deformation. 5. Wet snow. I. K.A. Shaw. II. G. Lemieux. III. United States. Army Cold Reg[illegible] Research and Engineering Laboratory, Hanover, N.H. [illegible]. Title III. Series

☆U.S. GOVERNMENT PRINTING OFFICE: 1977—702-611/25